This is an open access article published under a Creative Commons Attribution (CC-BY) License, which permits unrestricted use, distribution and reproduction in any medium, provided the author and source are cited.

ACS AUTHORCHOICE

ACS APPLIED ENERGY MATERIALS

www.acsaem.org Article

Benzo-Dipteridine Derivatives as Organic Cathodes for Li- and Na-ion Batteries

Michele Cariello,[‡] Beth Johnston,[‡] Manik Bhosale,[‡] Marco Amores,[‡] Emma Wilson, Liam J. McCarron, Claire Wilson, Serena A. Corr,* and Graeme Cooke*

Cite This: *ACS Appl. Energy Mater.* 2020, 3, 8302−8308

Read Online

ACCESS | Metrics & More | Article Recommendations | Supporting Information

ABSTRACT: Organic-based electrodes for Li- and Na-ion batteries present attractive alternatives to commonly applied inorganic counterparts which can often carry with them supply-chain risks, safety concerns with thermal runaway, and adverse environmental impact. The ability to chemically direct the structure of organic electrodes through control over functional groups is of particular importance, as this provides a route to fine-tune electrochemical performance parameters. Here, we report two benzo-dipteridine derivatives, **BF-Me$_2$** and **BF-H$_2$**, as high-capacity electrodes for use in Li- and Na-ion batteries. These moieties permit binding of multiple Li-ions per molecule while simultaneously ensuring low solubility in the supporting electrolyte, often a precluding issue with organic electrodes. Both display excellent electrochemical stability, with discharge capacities of 142 and 182 mAh g^{-1} after 100 cycles at a C/10 rate and Coulombic efficiencies of 96% and ∼ 100% demonstrated for **BF-Me$_2$** and **BF-H$_2$**, respectively. The application of a Na-ion cell has also been demonstrated, showing discharge capacities of 88.8 and 137 mAh g^{-1} after 100 cycles at a C/2 rate for **BF-Me$_2$** and **BF-H$_2$**, respectively. This work provides an encouraging precedent for these and related structures to provide versatile, high-energy density, and long cycle-life electrochemical energy storage materials.

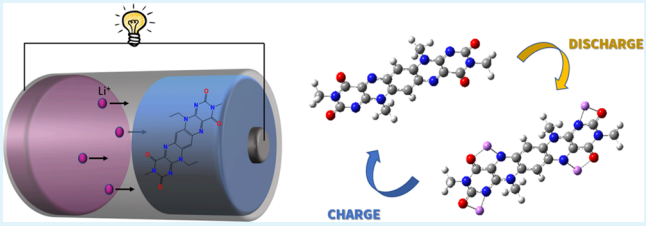

KEYWORDS: *organic electrodes, Li-ion battery, Na-ion battery, flavin cathodes*

Lithium ion (Li-ion) batteries continue to find their application in the electric vehicle market and as efficient energy storage systems for energy derived from intermittent power sources (e.g., tidal, solar, and wind).[1] Traditionally, positive electrodes in Li-ion batteries have been fabricated from metal-based inorganic materials.[2−5] However, there has been increasing interest in rechargeable batteries featuring redox-active organic molecules[6,7] as alternatives to current commercial active electrodes. This has largely resulted from their lower environmental impact, improved sustainability, and ability to conveniently tune their redox properties through synthetic manipulation.[6−11] However, the future development of Li-ion batteries based on organic electrodes presents several challenges as they must satisfy stringent requirements, which include: low solubility in conventional electrolytes, the ability to reversibly bind lithium ions, and good electrical conductivity. These systems should also have properties comparable to inorganic batteries. For example, organic electrodes often display declining voltage profiles upon repeated cycling, can exhibit solubility in the electrolyte, and have the propensity to participate in unwanted side reactions during battery cycling.[12−16] Therefore, the development of new materials with more favorable voltage profiles, good cycling kinetics, and improved cyclability is vital for the realization of high-performance organic-based batteries.

A biological system which shows great promise for organic electrodes is the flavins.[17,18] Flavins are pteridine-based derivatives containing a redox-active diazabutadiene nucleus and are ubiquitous biological redox cofactors for a number of biotransformations and energy transfer reactions.[19] Their redox-active nature has earmarked these compounds as attractive materials for the development of redox flow and Li-ion batteries. For example, Meng and co-workers used flavin mononucleotide (FMN) as a negative electrolyte in redox flow batteries (RFBs), achieving devices with stable performances over 100 cycles.[20] More recently, Aziz, Gordon, and co-workers have investigated the addition of solubilizing groups to an alloxazine core. The 7/8-carboxy-functionalized system produced RFBs with high current efficiency and capacity retention and open-circuit voltages approaching 1.2 V.[21]

With regard to Li-ion batteries, Kang, Park, and co-workers have employed riboflavin and lumiflavin as cathodes, demonstrating that Li-ion binding occurs similar to H$^+$ binding

Received: April 14, 2020
Accepted: July 30, 2020
Published: August 18, 2020

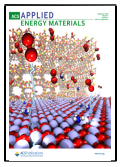

© 2020 American Chemical Society

https://dx.doi.org/10.1021/acsaem.0c00829
ACS Appl. Energy Mater. 2020, 3, 8302−8308

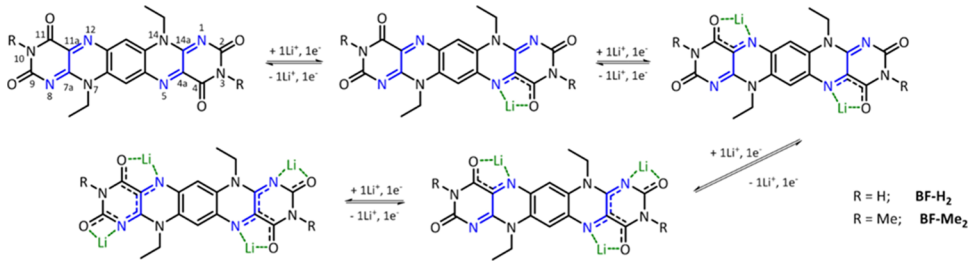

Figure 1. Chemical structure of benzo-dipteridine derivatives **BF-Me$_2$** and **BF-H$_2$** and potential reaction mechanism with lithium.

during the natural reduction of riboflavin, and have achieved capacities of around 174 mAh g^{-1} for lumiflavin and 105 mAh g^{-1} for riboflavin.[22] Park, Kang, and co-workers investigated the role the submoieties that form the flavin unit play in the battery characteristics.[11] Simplifying the flavin structure to alloxazine and lumazine improved the energy density; however, the smaller structures promoted higher solubility in the electrolyte. The incorporation of single-walled carbon nanotubes (SWCNTs) expanded and improved the use of alloxazine and lumazine derivatives for Li-ion batteries. Anchoring riboflavin and lumiflavin to SWCNTs resulted in a significant enhancement in the specific capacity, rate capability, and cyclability of Li-ion batteries.[23] Flavins have also been previously employed as pendant groups on poly(norbornene) polymer electrodes, where initial discharge capacities of 125 mAh g^{-1} at a C/10 rate are obtained for this hierarchical structure, which was employed to limit the solubility of the system in the electrolyte.[24] Nevertheless, significant capacity fading was still observed, suggesting that other degradation mechanisms also occur. Cho and co-workers reported the use of 7,8-dimethylalloxazine (or lumichrome) as the cathode material in Li-ion pouch cells, which displayed initial discharge capacities of ∼140 mAh g^{-1} similar to those observed for coin cells.[25]

Although biomimetic flavins have been mainly used in these studies, nonnatural synthetic flavins[26] offer the prospect of superior materials for use as active electrodes due to the ability to tune their redox, solubility, and structural properties through synthetic manipulation.[27,28] Here, we present a series of *bis*-flavin-like benzo-dipteridine derivatives **BF-Me$_2$** and **BF-H$_2$** (Figure 1) as a new generation of organic battery materials. Benzo-dipteridines[29] have been selected for this study due to their very poor solubility in most solvents, their ability to form π-stacked structures,[30] and their propensity to undergo multiple, reversible one-electron reductions due to the presence of two diazabutadiene moieties (labeled in blue in Figure 1), which can accommodate up to two electrons.[31] Similar to riboflavin, subsequent lithium insertion would be favored by carbonyl groups next to active nitrogen atoms, as they provide stabilization of the lithiated complex by chelation. Furthermore, the presence of two electron-withdrawing pteridine cores shifts the redox potential toward more negative values than that of the corresponding flavin analogs, leading to possible exploitation of larger potential windows and higher theoretical capacities compared to flavins. Another major advantage offered by this system is its great structural versatility. For instance, the choice of alkyl chains on the N3, N7, N10, and N14 positions has a considerable impact on the solubility and chelation properties of the resulting organic electrode. Here, we report the electrochemical performance of **BF-Me$_2$** and **BF-H$_2$**, demonstrating high capacities and excellent capacity retention after 100 cycles, and we apply the insights from density functional theory (DFT) to explain stability over repeated cycling.

The synthesis of **BF-Me$_2$** was carried out according to that previously reported by Yano et al. (Scheme S1).[32] Commercially available *p*-aminoaniline **1** was first acylated and then reduced to obtain *bis*-aniline **3** in nearly quantitative yield for both steps. This was made to react with 6-chloro-3-methyluracil to afford compound **4**, which, after nitration, underwent ring-closure, forming 5,12-di-*N*-oxide, which was deoxygenated to afford **BF-Me$_2$**. Similarly, **BF-H$_2$** (Scheme S2) was obtained by reacting **3** with 6-chlorouracil, affording **5**, which underwent nitration and ring-closure under the same conditions. The deoxygenation reaction required a much higher dilution due to higher insolubility of the parent 5,12-*N*-dioxide. A detailed description of the synthetic routes for both **BF-Me$_2$** and **BF-H$_2$** is provided in the Supporting Information. The X-ray crystal structure was obtained for **BF-Me$_2$**, confirming the linear structure. A full description can be found in the Supporting Information.

To assess the potential of lithium binding in these molecules, a series of DFT calculations were performed.[33] To computationally predict the most likely energetically favorable sites for lithiation, **BF-Me$_2$** was first geometrically optimized and then a lithium atom was placed at different sites at an approximate 4 Å distance from the molecule to allow the system to geometrically rearrange to the most energetically favorable state. The same calculations were also performed on **BF-H$_2$** and the results are reported in the Supporting Information. Figure 2 shows the most stable structures for

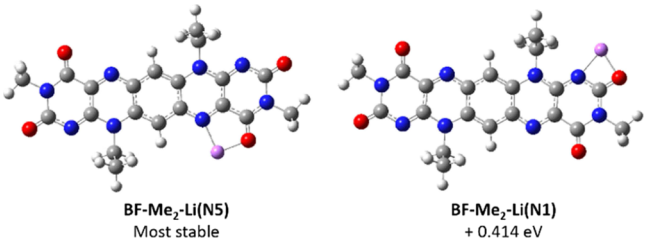

Figure 2. Molecular structure of the calculated most stable conformations of **BF-Me$_2$**, after a single-electron reduction and lithium binding. Of these, **BF-Me$_2$-Li(N5)** was found to be more stable than **BF-Me$_2$-Li(N1)** by 0.414 eV.

the monolithiated **BF-Me$_2$**, **BF-Me$_2$-Li(N5)**, and **BF-Me$_2$-Li(N1)**, where the former is thermodynamically more favorable by 0.414 eV. This energy difference is likely due to the stabilizing action of the lithium ion on the radical anion of **BF-Me$_2$**. Figure 3 shows a DFT-calculated radical map of the one-electron reduced **BF-Me$_2$** (top). The addition of a lithium ion does not drastically affect the radical distribution (bottom),

https://dx.doi.org/10.1021/acsaem.0c00829
ACS Appl. Energy Mater. 2020, 3, 8302−8308

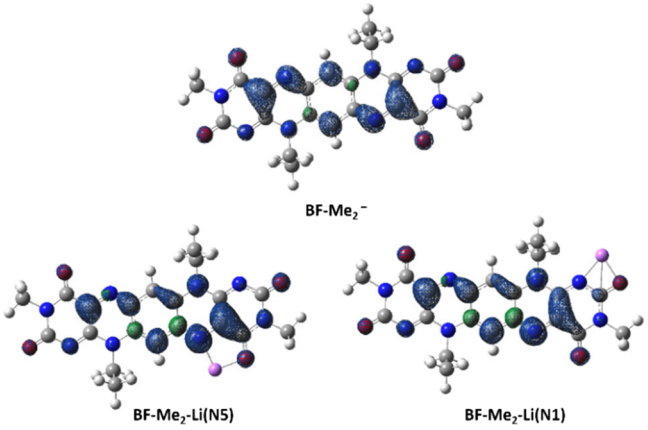

Figure 3. Radical distribution maps for one-electron reduced **BF-Me$_2^-$** and the monolithiated species **BF-Me$_2$-Li(N5)** and **BF-Me$_2$-Li(N1)**.

which remains localized on C4a and N5, suggesting that the electrostatic interaction between the unpaired electron and Li^+ at N5 would be stronger than that between Li^+ and N1.

Similarly, another lithium ion was added to the two monolithiated species and the four most stable conformations were obtained (Figure S5, Supporting Information). As expected from symmetry considerations, the twofold reduced dipteridine with lithium ions at N5 and N12, **BF-Me$_2$-Li2(N5, N12)** is the most energetically favorable conformation. Furthermore, **BF-Me$_2$-Li2(N5, N12)** is the most planar of the four conformations, while the least stable **BF-Me$_2$-Li2(N5, N1)** shows a more bent structure, with a dihedral angle of 6° between the fully lithiated pteridine and its fully oxidized counterpart. Figure 4 shows an indication of how the planarity of **BF-Me$_2$** changes upon full reduction and lithiation. The low solubility of the fully oxidized dipteridine can be explained based on the formation of strong intermolecular π-π stacking interactions, enhanced by the high planarity of the molecule and the low steric hindrance of the side-chains. Upon lithiation, the molecule progressively bends toward a chair-like configuration. This geometric rearrangement is more evident upon the third and fourth lithiations, with the plane of the core moiety twisted by approximately 7° and 11°, respectively, with respect to the phenyl center. This structural rearrangement is also evident by comparing the bond distances before and after lithiation (Table S1, Supporting Information). Upon lithiation, the C═O and C═N bonds are stretched, which led to progressive loss of their sp^2 character and therefore the ability to form intermolecular π stacks. An almost identical result was observed for **BF-H$_2$** with the same structural rearrangement to a chair-like configuration upon lithiation and bond distances very similar to those of **BF-Me$_2$** (Table S2, Supporting Information).

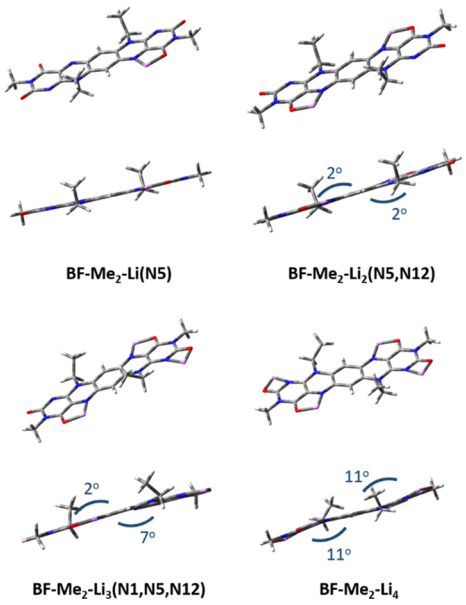

Figure 4. Geometry comparison between **BF-Me$_2$** and **BF-Me$_2$-Li$_4$**.

To investigate the electrochemical performance of **BF-H$_2$** and **BF-Me$_2$**, galvanostatic cycling experiments were performed in Swagelok-type cells using two different electrolyte systems: 1 M $LiPF_6$ in EC:DMC (vol 1:1) (carbonate-based) and 1 M lithium *bis*(trifluoromethanesulfonyl)imide (LiTFSI) in dioxolane (DOL):dimethoxyethane (DME) (vol 1:1) (ether-based). The theoretical capacities of **BF-H$_2$** and **BF-Me$_2$** are calculated to be 263 and 247 mAh g^{-1}, respectively, assuming that four Li-ions can be associated with each molecule during one redox cycle. For cells cycled at a C/10 rate within a voltage window of 1.2−4.0 V in 1 M $LiPF_6$ in EC:DMC, it can be observed in the Supporting Information (Figure S6) that this theoretical capacity is exceeded for both compounds during their first cycle. This indicates additional processes beyond the four Li^+ ions expected from stoichiometry and DFT predictions.

The redox activity of both materials was confirmed by CV, with a series of anodic and cathodic peaks observed (Figure 5a,b). For **BF-Me$_2$**, a reduction peak is initially observed at ca.

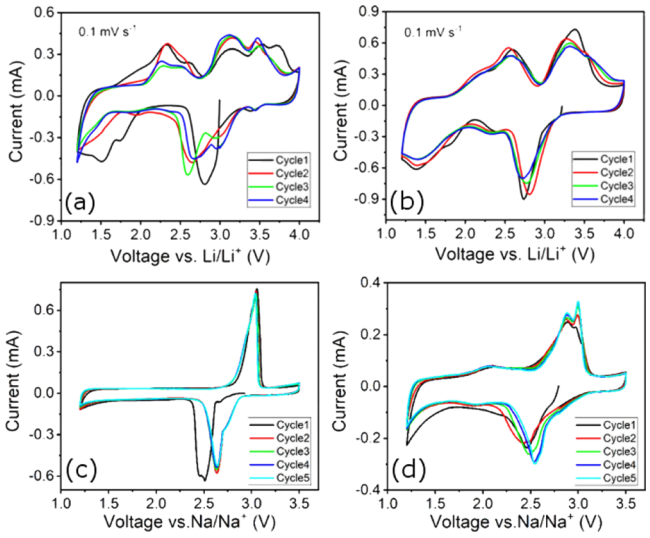

Figure 5. Cyclic voltammograms for charge−discharge cycles of (a) **BF-Me$_2$** and (b) **BF-H$_2$** measured at a scan rate of 0.1 mV s^{-1} between 1.2 and 4.0 V vs Li/Li^+ and (c) **BF-Me$_2$** and (d) **BF-H$_2$** measured at a scan rate of 0.1 mV s^{-1} between 1.2 and 3.5 V vs Na/Na^+.

2.8 V versus Li/Li^+ which can be attributed to the first and second Li^+ ions binding to equivalent sites within the molecule (Figure 5a). This peak splits upon further cycling, which may indicate that the previously equivalent sites have been slightly changed. As the voltage is swept from low to higher values, oxidation peaks are observed at 2.3, 3.1, and 3.5 V versus Li/

https://dx.doi.org/10.1021/acsaem.0c00829
ACS Appl. Energy Mater. 2020, 3, 8302−8308

Li^+. The peak at 2.3 V is split, which indicates that a 2 Li^+ removal process occurs on nearly equivalent sites. The further two peaks most likely arise from the consecutive removal of the remaining Li^+ ions in order to achieve full oxidation of the dipteridine unit. Figure S8 shows the comparison of the first cycle CV and the dQ/dV plot, in addition to dQ/dV data across the first four cycles, where a peak between 1.5 and 1.6 V versus Li/Li^+ is observed, and shows little change in intensity and position across cycling. This peak is most likely attributed to the capacity delivered during the binding of the final two Li^+ ions to the **BF-H$_2$** molecule, resulting in a full reduction of the unit. Thus, taking into account the peak shifts observed between the CV and dQ/dV profiles, it is reasonable to assume that the peak at 1.5 V observed in the CV profile can be assigned to the aforementioned Li^+ binding.

For **BF-H$_2$**, there is a markedly improved overlap of peaks for consecutive cycles in the carbonate-based electrolyte (Figure 5b). For example, the reduction peak at 2.8 V, likely corresponding to the binding of the first two Li^+ ions on the N5 and N12 sites, experiences very little voltage shift upon further cycling and there is no splitting of this peak. Oxidation peaks for this compound are observed at around 2.6 and 3.3 V versus Li/Li^+, with each peak indicating a 2 Li^+ ion removal process. The cycling stability of both **BF-Me$_2$** and **BF-H$_2$** decreased with an increased cycle number, indicating the possible dissolution of active materials in the carbonate-based electrolyte. To mitigate this effect, further cycling experiments were performed in an ether-based electrolyte (Figure 6). At a C/10 rate, a capacity of 182 mAh g^{-1} is observed even after 100 cycles with almost 100% Coulombic efficiency for **BF-H$_2$** (Figure 6b,d). Similarly, **BF-Me$_2$** displays its best performance in an ether-based electrolyte within a potential window of 1.35−4.00 V with a discharge capacity of 142 mAh g^{-1} observed after 100 cycles at C/10 rate with a Coulombic efficiency of 96% (Figure 6a,c).

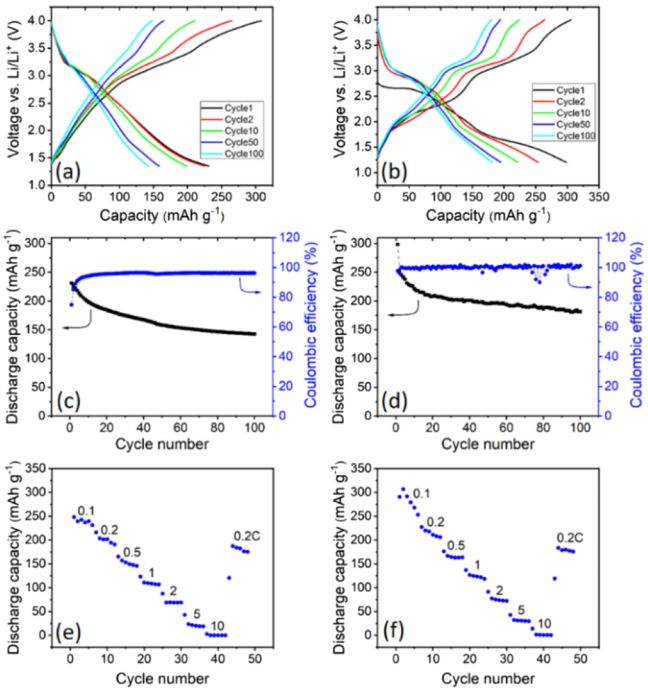

Figure 6. Cycling performance for the 1st, 2nd, 10th, 50th, and 100th cycle and cycling stabilities and Coulombic efficiencies for (a), (c) **BF-Me$_2$** between 1.35 and 4.0 V and (b), (d) **BF-H$_2$** between 1.2 and 4.0 V vs Li/Li^+ at a rate of C/10 in an ether-based electrolyte. Rate performance of (e) **BF-Me$_2$** and (f) **BF-H$_2$** measured at a different C rate from C/10 to 10C.

The rate performance of the **BF-Me$_2$** and **BF-H$_2$** pressed pellet electrodes (see the Supporting Information) was measured at increasing C-rates from C/10 to 10C, as shown in Figure 6e,f. As the charge/discharge current increases, both electrodes exhibit excellent capacity retention. A capacity retention of over 180 mAh g^{-1} at a C/5 rate is observed in both the cases. The rate performance of the **BF-Me$_2$** and **BF-H$_2$** electrode films was also measured at various C-rates from C/10 to 10C, and these results are shown in the Supporting Information (Figure S9). Interestingly, even at a rate of 10C, the **BF-H$_2$** material displays a discharge capacity of 127 mAh g^{-1} (75 mAh g^{-1} in the case of **BF-Me$_2$**). These materials show excellent cycling stability and high rate performance likely due to their high conjugation and planar geometry. As DFT studies suggest, upon lithiation, both molecules have the tendency to bend into a chair-like configuration, therefore weakening the π-stacking interactions, which could, in turn, contribute to an increase in the solubility of the compounds in the organic electrolyte. However, unlike **BF-Me$_2$**, the lack of functionalization on N3 and N10 in **BF-H$_2$** provides an opportunity for H-bond formation, which would decrease the solubility of this compound compared to its dimethylated counterpart. This has obvious implications on electrochemical performance as one would expect less severe degradation effects for this bent conformation. The formation of H-bonds in N3 unfunctionalized isoalloxazines with diaminopyridine derivatives, acting as flavin receptors, has been widely reported in the literature.[26,28,34,35] Moreover, Ohshiro et al. demonstrated the formation of a charge-transfer complex between two N3 and N10 unfunctionalized dipteridine molecules having different oxidation states, interacting with each other through antiparallel dipoles (N−H and C═O).[30]

To further examine the lithiation mechanisms in **BF-Me$_2$** and **BF-H$_2$**, ex situ ATR-IR spectroscopy and X-ray diffraction measurements were performed on each cathode material prior to cycling, upon discharge to 1.2 V and after subsequent charging to 4 V (see the Supporting Information for experimental details). ATR-IR is particularly useful in examining vibrational energy levels to assess changes during electrochemical cycling, as exemplified by recent developments in operando measurements by Bitenc et al.[36] The benzodipteridine derivatives **BF-Me$_2$** and **BF-H$_2$** possess several characteristic IR bands, including C═O stretches (∼1715−1730 and ∼ 1680 cm^{-1}) and the vibrational mode from N4 = C4a−C14a = N4 (shown in blue in Figure 1) which are sensitive to reduction.[37] Spectra recorded for both compounds upon discharge show a weakening and negative shift in the C═O stretches (Figure S10), indicating a reduction of these groups in good agreement with the proposed mechanism as shown in Figure 1. These peaks re-emerge upon charging, demonstrating the reversibility of this process. Ex situ X-ray diffraction data collected for both materials after discharge and upon recharge show a high degree of amorphization (Figure S11), similar to the behavior noted for the perylene anhydride electrode in K-ion batteries.[38] SEM images collected of the pristine material and the cathode prior to and after cycling confirm this loss of long-range crystallinity and a pronounced change in morphology (Figures S12-S17), where micron-long

https://dx.doi.org/10.1021/acsaem.0c00829
ACS Appl. Energy Mater. 2020, 3, 8302−8308

rod-shaped particles for pristine **BF-Me$_2$** and **BF-H$_2$** are broken down to smaller quasi-spherical particles postcycling.

The limited natural abundance of lithium has spurred investigations to find more sustainable carrier ions for rechargeable batteries with sodium emerging as a popular choice.[39] Therefore, we have investigated the cathode behavior of **BF-Me$_2$** and **BF-H$_2$** for rechargeable sodium-ion (Na-ion) batteries. Cyclic voltammograms for **BF-Me$_2$** and **BF-H$_2$** versus a sodium metal anode are shown in Figure 5c,d, respectively. Figure 5c shows the first five cycles of the CV curves of **BF-Me$_2$** in 1 M $NaPF_6$ in diethylene glycol dimethyl ether. In the first cathodic scan, there is a large reduction peak centered at ~2.5 V versus Na/Na^+, which appears at a lower potential compared with subsequent scans. This is reminiscent of the behavior observed for perylene diimide as a Na-ion cathode, where a large polarization was required for initial Na-ion insertion.[40] The reversed anodic scan shows a broad oxidation peak, with a shoulder, centered at ~2.9 V. The excellent reversibility is reflected by no changes in peak positions or intensities in subsequent cycles. In the case of **BF-H$_2$** (Figure 5d), a broad reduction peak is observed at 2.45 V versus Na/Na^+ in the first scan with two oxidation peaks found in the anodic scans at 2.8 and 3.0 V. On subsequent scans, a slight shift to higher potentials is again observed, indicating an increasing polarization. The overlap in peak position and intensity in later scans indicates good electrochemical reversibility. Cycling studies were carried out for both electrodes at a C/10 rate. For **BF-Me$_2$**, an initial discharge capacity of 160 mAh g^{-1} is observed, which reduces to 125 mAh g^{-1} after 25 cycles. The **BF-H$_2$** cathode displays a first discharge capacity of 240 mAh g^{-1} reducing to 153 mAh g^{-1} in the 25th cycle. A large difference between the first and second discharge capacities is attributed to reactions with the electrolyte. The cycling stability was examined at a C/2 rate for **BF-Me$_2$** and **BF-H$_2$**. The first and 100th cycle discharge capacities for the **BF-Me$_2$** electrode were 128.8 and 88.8 mAh g^{-1}, respectively, with a 100% Coulombic efficiency observed. For **BF-H$_2$**, the first discharge capacity was found to be 175 mAh g^{-1} at a C/2 rate, reducing to 137 mAh g^{-1} after 100 cycles with almost 100% Coulombic efficiency. The rate performance for both materials was determined at current densities ranging from C/10 to 10C. On final return to a C/10 rate, **BF-Me$_2$** and **BF-H$_2$** showed discharge capacities of 128 and 174 mAh g^{-1}, respectively, demonstrating good material stability at high current (Figures S18 and S19). Although improvements in cell construction, conductive carbon additives, and electrolyte optimization can lead to enhanced performance and are ongoing for these dipteridine compounds, these results demonstrate the promising application of **BF-Me$_2$** and **BF-H$_2$** as electrodes for both Li- and Na-ion batteries.[41,42] Overall, the electrochemical performances reported in this work were outstanding when compared across a variety of organic cathodes, thus achieving comparatively high discharge capacities and cycling stabilities for both lithium and sodium cells.[43−46]

Strong sharp redox peaks (corresponding to plateau-like features in the voltage profile in the galvanostatic cycling data) at around 2.8−3.4 V versus Li/Li^+ (Figure S20a) and 2.7−3.0 V vs Na/Na^+ (Figure S20b) indicate a two-phase reaction mechanism. In the case of the Li-ion cells, there are additional broad redox contributions over the rest of the cycled voltage window, which may be arising from solid-solution processes where Li-ions diffuse within the dipteridine material without producing a phase change. This type of redox reaction is absent in the Na-ion cells, indicating only a two-phase mechanism for these cells. This is in contrast to the Li-ion case where additional capacity arises as a result of the solid-solution mechanism. The additional solid-solution processes observed in the low-voltage regime are also more evident and contribute to a higher capacity in the case of the **BF-H$_2$** material, which indicates a less hindered ion diffusion compared to the bulkier methyl substituents of **BF-Me$_2$**, where steric hindrance may hamper ion diffusion.

In conclusion, we have reported the synthesis of two benzodipteridine derivatives, which show great promise for use as cathode materials for Li- and Na-ion batteries. We have shown that each molecule can accommodate at least four lithium ions, with high capacities and excellent cyclability demonstrated. **BF-Me$_2$** displays lower cycling stability compared to **BF-H$_2$**, which likely arises from the *N*-methyl group, preventing intermolecular H-bonding. Furthermore, the DFT-predicted loss of planarity, which affects both molecules upon lithiation, will likely result in increased solubility in the electrolyte due to the disruption of intermolecular π-π stacking interactions. The combination of DFT calculations with electrochemical experiments provides unique insights into the structure−property relationships of these organic electrodes, permitting future tailoring of the primary structure to avoid degradation through solubility effects. Without the need for postprocessing of the flavin moieties, these cathodes deliver high discharge capacities stable even after 100 cycles. This work paves the way for the incorporation of these materials and their molecularly engineered counterparts[47] into a range of cathode structures for Li- and Na-ion batteries.

■ ASSOCIATED CONTENT

Supporting Information

The Supporting Information is available free of charge at https://pubs.acs.org/doi/10.1021/acsaem.0c00829.

Detailed synthetic procedures, NMR characterization, crystallographic data, DFT modeling, electrode preparation, and battery characterization (PDF)

■ AUTHOR INFORMATION

Corresponding Authors

Serena A. Corr − *Department of Chemical and Biological Engineering and Department of Materials Science and Engineering, University of Sheffield, Sheffield S1 3JD, United Kingdom;* orcid.org/0000-0002-9303-4220; Email: s.corr@sheffield.ac.uk

Graeme Cooke − *School of Chemistry, University of Glasgow, Glasgow G12 8QQ, United Kingdom;* orcid.org/0000-0003-0890-5720; Email: Graeme.Cooke@Glasgow.ac.uk

Authors

Michele Cariello − *School of Chemistry, University of Glasgow, Glasgow G12 8QQ, United Kingdom*

Beth Johnston − *Department of Chemical and Biological Engineering, University of Sheffield, Sheffield S1 3JD, United Kingdom*

Manik Bhosale − *Department of Chemical and Biological Engineering, University of Sheffield, Sheffield S1 3JD, United Kingdom*

https://dx.doi.org/10.1021/acsaem.0c00829
ACS Appl. Energy Mater. 2020, 3, 8302−8308

Marco Amores − *Department of Chemical and Biological Engineering, University of Sheffield, Sheffield S1 3JD, United Kingdom;* orcid.org/0000-0002-0856-7453
Emma Wilson − *School of Chemistry, University of Glasgow, Glasgow G12 8QQ, United Kingdom*
Liam J. McCarron − *School of Chemistry, University of Glasgow, Glasgow G12 8QQ, United Kingdom*
Claire Wilson − *School of Chemistry, University of Glasgow, Glasgow G12 8QQ, United Kingdom;* orcid.org/0000-0002-0090-5374

Complete contact information is available at: https://pubs.acs.org/10.1021/acsaem.0c00829

Author Contributions

‡M.C., B.J., M.B., and M.A. contributed equally.

Funding

G.C. and S.C. thank the Supergen hub and EPSRC (EP/P00315X/1) for funding. S.C., M.B., B.J., and M.A. gratefully acknowledge the support of the University of Sheffield in our research, as well as grant support from the EPSRC [EP/N001982/2]. B.J. also gratefully acknowledges the award of a Carnegie PhD scholarship.

Notes

The authors declare no competing financial interest.

Materials supporting this paper can be accessed at http://dx.doi.org/10.5525/gla.researchdata.1046. The supplementary crystallographic data for this paper is listed under CCDC 1973257 and can be obtained free of charge from The Cambridge Crystallographic Data Centre at http://www.ccdc.cam.ac.uk/structures.

■ ACKNOWLEDGMENTS

G.C. and M.C. thank the EPSRC National Mass Spectrometry Facility (Singleton Park, Swansea, U.K.) for acquiring MS data and EPSRC UK National Crystallography Service at the University of Southampton for the collection of the crystallographic data.

■ REFERENCES

(1) Adelhelm, P. Editorial: The Energy Challenge, Batteries, and Why Simple Math Matters. *Angew. Chem., Int. Ed.* **2018**, *57*, 6710−6711.
(2) Wen, J.; Yu, Y.; Chen, C. A Review on Lithium-Ion Batteries Safety Issues: Existing Problems and Possible Solutions. *Mater. Express* **2012**, *2*, 197−212.
(3) Goodenough, J. B.; Park, K.-S. The Li-Ion Rechargeable Battery: A Perspective. *J. Am. Chem. Soc.* **2013**, *135*, 1167−1176.
(4) Daniel, C. Materials and processing for lithium-ion batteries. *JOM* **2008**, *60*, 43−48.
(5) Croy, J. R.; Abouimrane, A.; Zhang, Z. Next-generation lithium-ion batteries: The promise of near-term advancements. *MRS Bull.* **2014**, *39*, 407−415.
(6) Bhosale, M. E.; Chae, S.; Kim, J. M.; Choi, J.-Y. Organic small molecules and polymers as an electrode material for rechargeable lithium ion batteries. *J. Mater. Chem. A* **2018**, *6*, 19885−19911.
(7) Mauger, A.; Julien, C.; Paolella, A.; Armand, M.; Zaghib, K. Recent Progress on Organic Electrodes Materials for Rechargeable Batteries and Supercapacitors. *Materials* **2019**, *12*, 1770.
(8) Xie, J.; Zhang, Q. Recent progress in rechargeable lithium batteries with organic materials as promising electrodes. *J. Mater. Chem. A* **2016**, *4*, 7091−7106.
(9) Schon, T. B.; McAllister, B. T.; Li, P.-F.; Seferos, D. S. The rise of organic electrode materials for energy storage. *Chem. Soc. Rev.* **2016**, *45*, 6345−6404.
(10) Luo, C.; Borodin, O.; Ji, X.; Hou, S.; Gaskell, K. J.; Fan, X.; Chen, J.; Deng, T.; Wang, R.; Jiang, J.; Wang, C. Azo compounds as a family of organic electrode materials for alkali-ion batteries. *PNAS* **2018**, *115*, 2004−2009.
(11) Hong, J.; Lee, M.; Lee, B.; Seo, D.-H.; Park, C. B.; Kang, K. Biologically inspired pteridine redox centres for rechargeable batteries. *Nature Commun.* **2014**, *5*, 5335.
(12) Zou, Q.; Wang, W.; Wang, A.; Yu, Z.; Yuan, K. Preparation of the tetrahydro-hexaquinone as a novel cathode material for rechargeable lithium batteries. *Mater. Lett.* **2014**, *117*, 290−293.
(13) Nokami, T.; Matsuo, T.; Inatomi, Y.; Hojo, N.; Tsukagoshi, T.; Yoshizawa, H.; Shimizu, A.; Kuramoto, H.; Komae, K.; Tsuyama, H.; Yoshida, J.-I. Polymer-Bound Pyrene-4,5,9,10-tetraone for Fast-Charge and -Discharge Lithium-Ion Batteries with High Capacity. *J. Am. Chem. Soc.* **2012**, *134*, 19694−19700.
(14) Vadehra, G. S.; Maloney, R. P.; Garcia-Garibay, M. A.; Dunn, B. Naphthalene Diimide Based Materials with Adjustable Redox Potentials: Evaluation for Organic Lithium-Ion Batteries. *Chem. Mater.* **2014**, *26*, 7151−7157.
(15) Iordache, A.; Maurel, V.; Mouesca, J. M.; Pecaut, J.; Dubois, L.; Gutel, T. Monothioanthraquinone as an organic active material for greener lithium batteries. *J. Power Sources* **2014**, *267*, 553−559.
(16) Häupler, B.; Hagemann, T.; Friebe, C.; Wild, A.; Schubert, U. S. Dithiophenedione-Containing Polymers for Battery Application. *ACS Appl. Mater. Interfaces* **2015**, *7*, 3473−3479.
(17) Lee, B.; Ko, Y.; Kwon, G.; Lee, S.; Ku, K.; Kim, J.; Kang, K. Exploiting Biological Systems: Toward Eco-Friendly and High-Efficiency Rechargeable Batteries. *Joule* **2018**, *2*, 61−75.
(18) Wang, H.; Yang, Y.; Guo, L. Renewable-Biomolecule-Based Electrochemical Energy-Storage Materials. *Adv. Energy Mater.* **2017**, *7*, 1700663.
(19) Walsh, C. T.; Wencewicz, T. A. Flavoenzymes: versatile catalysts in biosynthetic pathways. *Nat. Prod. Rep.* **2013**, *30*, 175−200.
(20) Orita, A.; Verde, M. G.; Sakai, M.; Meng, Y. S. A biomimetic redox flow battery based on flavin mononucleotide. *Nature Commun.* **2016**, *7*, 13230.
(21) Lin, K.; Gómez-Bombarelli, R.; Beh, E. S.; Tong, L.; Chen, Q.; Valle, A.; Aspuru-Guzik, A.; Aziz, M. J.; Gordon, R. G. A redox-flow battery with an alloxazine-based organic electrolyte. *Nat. Energy* **2016**, *1*, 16102.
(22) Lee, M.; Hong, J.; Seo, D.-H.; Nam, D. H.; Nam, K. T.; Kang, K.; Park, C. B. Redox Cofactor from Biological Energy Transduction as Molecularly Tunable Energy-Storage Compound. *Angew. Chem., Int. Ed.* **2013**, *52*, 8322−8328.
(23) Lee, M.; Hong, J.; Kim, H.; Lim, H.-D.; Cho, S. B.; Kang, K.; Park, C. B. Organic Nanohybrids for Fast and Sustainable Energy Storage. *Adv. Mater.* **2014**, *26*, 2558−2565.
(24) Schon, T. B.; Tilley, A. J.; Bridges, C. R.; Miltenburg, M. B.; Seferos, D. S. Bio-Derived Polymers for Sustainable Lithium-Ion Batteries. *Adv. Funct. Mater.* **2016**, *26*, 6896−6903.
(25) Yeo, J.-S.; Yoo, E.-J.; Ha, S.-H.; Cheong, D.-I.; Cho, S.-B. Electrochemical properties of large-sized pouch-type lithium ion batteries with bio-inspired organic cathode materials. *J. Power Sources* **2016**, *313*, 91−95.
(26) Nandwana, V.; Samuel, I.; Cooke, G.; Rotello, V. M. Aromatic Stacking Interactions in Flavin Model Systems. *Acc. Chemi. Res.* **2013**, *46*, 1000−1009.
(27) Hasford, J. J.; Rizzo, C. J. Linear Free Energy Substituent Effect on Flavin Redox Chemistry. *J. Am. Chem. Soc.* **1998**, *120*, 2251−2255.
(28) Legrand, Y.-M.; Gray, M.; Cooke, G.; Rotello, V. M. Model Systems for Flavoenzyme Activity: Relationships between Cofactor Structure, Binding and Redox Properties. *J. Am. Chem. Soc.* **2003**, *125*, 15789−15795.
(29) Yano, Y.; Nakazato, M.; Vasquez, R. E. A flavin mimic possessing strong oxidizing power due to electron delocalization: a benzo-dipteridine. *J. Chem. Soc., Chem. Commun.* **1985**, 226−227.
(30) Ohshiro, H.; Tamura, N.; Arai, A.; Yamaguchi, K.; Takanobu, M.; Tominami, T.; Kondo, S.-I.; Nabeshima, T.; Yano, Y.; Toyoda, J.; Nakasuji, K.; Heelis, P. F. A Novel Property of Reduced

Benzodipteridine toward Molecular Oxygen. *Heterocycles* **1998**, *48*, 627−630.

(31) Ohshiro, H.; Mitsui, K.; Ando, N.; Ohsawa, Y.; Koinuma, W.; Takahashi, H.; Kondo, S.-I.; Nabeshima, T.; Yano, Y. Oxidation-Active Flavin Models: Oxidation of α-Hydroxy Acids by Benzodipteridine Bearing Metal-Binding Site in the Presence of Divalent Metal Ion and Base in Organic Solvents. *J. Am. Chem. Soc.* **2001**, *123*, 2478−2486.

(32) Yoneda, F.; Koga, M.; Tanaka, K.; Yano, Y. Syntheses of 1,3,6,8,10,11,14-heptaazapentaphene-2,4,7,9(14H,3H,8H, -11H)-tetrones (angular mixed flavins), 1,3,5,6,8,10,11,14-octaazapentaphene-2,4,7,9(14H,3H,8H,11H)-tetrones (angular doubled flavins), and their related compounds. *J. Heterocycl. Chem.* **1989**, *26*, 1221−1228.

(33) Frisch, M. J.; Trucks, G. W.; Schlegel, H. B.; Scuseria, G. E.; Robb, M. A.; Cheeseman, J. R.; Scalmani, G.; Barone, V.; Mennucci, B.; Petersson, G. A.; Nakatsuji, H.; Caricato, M.; Li, X.; Hratchian, H. P.; Izmaylov, A. F.; Bloino, J.; Zheng, G.; Sonnenberg, J. L.; Hada, M.; Ehara, M.; Toyota, K.; Fukuda, R.; Hasegawa, J.; Ishida, M.; Nakajima, T.; Honda, Y.; Kitao, O.; Nakai, H.; Vreven, T.; Montgomery, Jr., J. A.; Peralta, J. E.; Ogliaro, F.; Bearpark, M. J.; Heyd, J.; Brothers, E. N.; Kudin, K. N.; Staroverov, V. N.; Kobayashi, R.; Normand, J.; Raghavachari, K.; Rendell, A. P.; Burant, J. C.; Iyengar, S. S.; Tomasi, J.; Cossi, M.; Rega, N.; Millam, N. J.; Klene, M.; Knox, J. E.; Cross, J. B.; Bakken, V.; Adamo, C.; Jaramillo, J.; Gomperts, R.; Stratmann, R. E.; Yazyev, O.; Austin, A. J.; Cammi, R.; Pomelli, C.; Ochterski, J. W.; Martin, R. L.; Morokuma, K.; Zakrzewski, V. G.; Voth, G. A.; Salvador, P.; Dannenberg, J. J.; Dapprich, S.; Daniels, A. D.; Farkas, Ö.; Foresman, J. B.; Ortiz, J. V.; Cioslowski, J.; Fox, D. J., *Gaussian 09*. Gaussian, Inc.: Wallingford, CT, USA, 2009.

(34) Yano, Y.; Tamura, N.; Mitsui, K.; Nabeshima, T. A Flavin Receptor. Effect of 2,6-Diaminopyridine Derivatives on the Reduction of Benzo-Dipteridine (Oxidation-Active Flavin Model). *Chem. Lett.* **1989**, *18*, 1655−1658.

(35) Tamura, N.; Mitsui, K.; Nabeshima, T.; Yano, Y. Synthesis of 2,6-diamidopyridine derivatives and their functions as flavin receptors in chloroform. *J. Chem. Soc., Perkin Trans. 2* **1994**, 2229−2237.

(36) Vizintin, A.; Bitenc, J.; Kopač Lautar, A.; Pirnat, K.; Grdadolnik, J.; Stare, J.; Randon-Vitanova, A.; Dominko, R. Probing electrochemical reactions in organic cathode materials via in operando infrared spectroscopy. *Nat. Commun.* **2018**, *9*, 661.

(37) Iuliano, J. N.; French, J. B.; Tonge, P. J., Vibrational spectroscopy of flavoproteins. In *Methods in Enzymology*, Palfey, B. A., Academic Press: 2019; *620*, 189−214.

(38) Xing, Z.; Jian, Z.; Luo, W.; Qi, Y.; Bommier, C.; Chong, E. S.; Li, Z.; Hu, L.; Ji, X. A perylene anhydride crystal as a reversible electrode for K-ion batteries. *Energy Storage Mater.* **2016**, *2*, 63−68.

(39) Kim, S.-W.; Seo, D.-H.; Ma, X.; Ceder, G.; Kang, K. Electrode Materials for Rechargeable Sodium-Ion Batteries: Potential Alternatives to Current Lithium-Ion Batteries. *Adv. Energy Mater.* **2012**, *2*, 710−721.

(40) Deng, W.; Shen, Y.; Qian, J.; Cao, Y.; Yang, H. A Perylene Diimide Crystal with High Capacity and Stable Cyclability for Na-Ion Batteries. *ACS Appl. Mater. Interfaces* **2015**, *7*, 21095−21099.

(41) Hu, Y.; Tang, W.; Yu, Q.; Yang, C.; Fan, C. In Situ Electrochemical Synthesis of Novel Lithium-Rich Organic Cathodes for All-Organic Li-Ion Full Batteries. *ACS Appl. Mater. Interfaces* **2019**, *11*, 32987−32993.

(42) Yao, Z.; Tang, W.; Wang, X.; Wang, C.; Yang, C.; Fan, C. Synthesis of 1,4-benzoquinone dimer as a high-capacity (501 mA h g−1) and high-energy-density (>1000 Wh kg−1) organic cathode for organic Li-Ion full batteries. *J. Power Sources* **2020**, *448*, 227456.

(43) Mumyatov, A. V.; Shestakov, A. F.; Dremova, N. N.; Stevenson, K. J.; Troshin, P. A. New Naphthalene-Based Polyimide as an Environment-Friendly Organic Cathode Material for Lithium Batteries. *Energy Technol.* **2019**, *7*, 1801016.

(44) Ba, Z.; Wang, Z.; Luo, M.; Li, H.-B.; Li, Y.; Huang, T.; Dong, J.; Zhang, Q.; Zhao, X. Benzoquinone-Based Polyimide Derivatives as High-Capacity and Stable Organic Cathodes for Lithium-Ion Batteries. *ACS Appl. Mater. Interfaces* **2020**, *12*, 807−817.

(45) Peterson, B. M.; Ren, D.; Shen, L.; Wu, Y.-C. M.; Ulgut, B.; Coates, G. W.; Abruña, H. D.; Fors, B. P. Phenothiazine-Based Polymer Cathode Materials with Ultrahigh Power Densities for Lithium Ion Batteries. *ACS Appl. Energy Mater.* **2018**, *1*, 3560−3564.

(46) Deng, W.; Yu, J.; Qian, Y.; Wang, R.; Ullah, Z.; Zhu, S.; Chen, M.; Li, W.; Guo, Y.; Li, Q.; Liu, L. Strongly coupled perylene bisimide/reduced graphene oxide as organic cathode materials for lithium ion batteries. *Electrochim. Acta* **2018**, *282*, 24−29.

(47) Kim, D. J.; Hermann, K. R.; Prokofjevs, A.; Otley, M. T.; Pezzato, C.; Owczarek, M.; Stoddart, J. F. Redox-Active Macrocycles for Organic Rechargeable Batteries. *J. Am. Chem. Soc.* **2017**, *139*, 6635−6643.

https://dx.doi.org/10.1021/acsaem.0c00829
ACS Appl. Energy Mater. 2020, 3, 8302−8308